Optics Letters

Nonlinear Fourier transform for characterization of the coherent structures in optical microresonators

Sergei K. Turitsyn,[1,2] Igor S. Chekhovskoy,[2,3,*] and Mikhail P. Fedoruk[2,3]

[1]Aston Institute of Photonic Technologies, Aston University, Birmingham B4 7ET, UK
[2]Aston-NSU Center for Photonics, Novosibirsk State University, Novosibirsk 630090, Russia
[3]Institute of Computational Technologies, SB RAS, Novosibirsk 630090, Russia
*Corresponding author: i.s.chekhovskoy@nsu.ru

Received 20 February 2020; revised 14 April 2020; accepted 20 April 2020; posted 21 April 2020 (Doc. ID 390630); published 27 May 2020

We propose and demonstrate, in the framework of the generic mean-field model, the application of the nonlinear Fourier transform (NFT) signal processing based on the Zakharov–Shabat spectral problem to the characterization of the round trip scale dynamics of radiation in optical fiber- and microresonators.

https://doi.org/10.1364/OL.390630

The nonlinear Fourier transform {known as the inverse scattering transform (IST) in the mathematical literature [1–3]} is a powerful method that has been invented and extensively used for the description of the solutions of the so-called integrable nonlinear partial differential equations. An important example of an integrable model is the nonlinear Schrödinger equation (NLSE) [2], which in the context of optics is related to the description of nonlinear propagation of light in optical fiber and many other applications. Recently, nonlinear Fourier transform (NFT) has been applied for the analysis of laser radiation [4–7]. We would like to stress that this a rather nontraditional application of the method, because conventionally, NFT is associated with the integrable conservative Hamiltonian models, while lasers are strongly dissipative systems and laser dissipative solitons substantially differ from solitons of the NLSE.

In Refs. [6,7] this concept was introduced, and it was demonstrated on several practical examples that compared to the conventional Fourier analysis, NFT might offer a description of optical pulses using a smaller number of variables (effective degrees of freedom) with acceptable accuracy. Here we apply this emerging signal processing technique for analysis of the dynamics of nonlinear structures in the fiber- or microresonators.

The master average model (here only anomalous dispersion) to describe the evolution of the slowly varying envelope of the optical field in nonlinear fiber- or microresonators {see for details [8–15] and references therein regarding the Lugiato–Lefever equation (LLE)} reads

$$i\frac{\partial \Psi}{\partial T}+\frac{1}{2}\frac{\partial^2 \Psi}{\partial \tau^2}+|\Psi|^2\Psi=(-i+\zeta_0)\,\Psi+if. \tag{1}$$

Here $\Psi(T,\tau)$ is a slowly varying field amplitude, T is a normalized slow time corresponding to the cavity round trips, τ is a dimensionless longitudinal coordinate related to the angular characteristic inside the microresonator (or the local time characteristic in case of fiber-resonator), ζ_0 is the normalized laser detuning between the pump laser frequency and the cold-cavity resonance frequency, and f is the normalized pump field amplitude. Equation (1) is a mean-field equation [16–18] widely known as the LLE, and the left-hand side of Eq. (1) presents the integrable NLSE [2]. Note that Eq. (1) was originally introduced and studied in the context of plasma physics in [16], and it was first derived in the temporal domain in Ref. [18].

A typical solution of Eq. (1) includes a CW background $\Psi_0(T)$ and a solitonic part $\Psi_1(T,\tau)$. The evolution of the CW background $\Psi_0(T)$ over resonator round trips is given by

$$i\frac{\partial \Psi_0}{\partial T}+|\Psi_0|^2\Psi_0=(-i+\zeta_0)\,\Psi_0+if. \tag{2}$$

There are well-known stationary solutions in the form of a constant CW background (see for details [8,10–13] and references therein) that can be found by solving Eq. (2) with $\frac{\partial \Psi_0}{\partial T}=0$, yielding algebraic equation on the stationary background ($I_0=|\Psi_0|^2$), $I_0^3-2\zeta_0 I_0^2+(1+\zeta_0^2)I_0-f^2=0$. The number of real roots is determined by the double inequality $f_-\le f\le f_+$, where $f_\pm^2=\frac{2}{27}(\zeta_0(\zeta_0^2+9)\pm\sqrt{(\zeta_0^2-3)^3})$. When f satisfies this inequality, there are three real roots (one root is unstable); otherwise, there is only one real root.

When localized structures have scale much less than the round trip (e.g., a single dissipative soliton or a set of solitons), it is possible to separate dynamics of the stable background field with nonzero boundary conditions (in τ) from the evolution of the localized in time (vanishing boundary conditions) soliton content. This is because at large τ, the localized soliton component does not affect the background. Considering the solution of the master model Eq. (1) as a sum of the uniform (in τ) background Ψ_0 that depends only on T and the soliton (localized in τ) component Ψ_1, we can separate the equation for Ψ_0 [Eq. (2)], and the equation governing dynamics of the function Ψ_1,

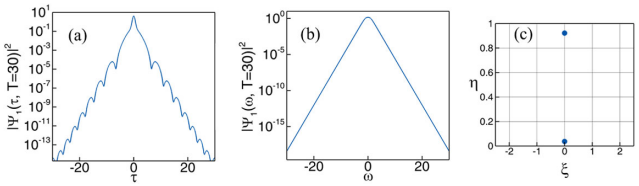

Fig. 1. Soliton solution in the case $\zeta_0 = 2$, $f = \sqrt{2}$, shown at $T = 30$, generated from the initial conditions $\Psi_0(T = 0) = 0$, $\Psi_1(\tau, T = 0) = \mathrm{sech}(\tau)$: (a) intensity profile, (b) soliton power spectrum, (c) nonlinear discrete spectrum of the formed dissipative soliton.

$$i\frac{\partial \Psi_1}{\partial T} + \frac{1}{2}\frac{\partial^2 \Psi_1}{\partial \tau^2} + |\Psi_1|^2\Psi_1 = R[\Psi_0, \Psi_1], \tag{3}$$

with the perturbative term R describing deviation of Eq. (3) from the integrable NLSE that is presented by the left-hand side of Eq. (3) having the form

$$R = (-i + \zeta_0)\,\Psi_1 - 2|\Psi_0|^2\Psi_1 - 2\Psi_0|\Psi_1|^2 - \Psi_0^2\Psi_1^* - \Psi_0^*\Psi_1^2. \tag{4}$$

However, we would like to stress that such an approach to separate the equations to the CW and solitonic parts only works when the CW part does not approach the unstable (due to the modulation instability) upper state.

The NLSE is integrable [2], and its solutions can be linked to the solution of the Zakharov–Shabat problem (ZSP) [2] for potential $\Psi_1(T, \tau)$ with a spectral parameter $\lambda = \xi + i\eta$,

$$\frac{\partial u}{\partial \tau} = -i\lambda u + \Psi_1(T, \tau)v, \quad \frac{\partial v}{\partial \tau} = -\Psi_1^*(T, \tau)u + i\lambda v. \tag{5}$$

We consider here localized fields $\Psi_1(T, \tau)$ with vanishing boundary conditions at $\tau \to \pm\infty$. The spectral parameter λ defines nonlinear spectra associated with the field $\Psi_1(T, \tau)$. All details can be found in [2,3,19]; therefore, we only briefly remind here the key points. The complete NFT spectrum of the considered ZSP includes the following: (i) a continuous spectrum that is defined on the real axis of the complex plane $Re(\lambda) = \xi$ by the complex function $r(\xi) = b(\xi)/a(\xi)$, where $a(\xi)$ and $b(\xi)$ are the so-called Jost coefficients, which are computed using ZSP [Eq. (5)]; and (ii) a discrete spectrum that is given by $4 \times N$ real parameters (the set of complex-valued eigenvalues $\{\lambda_n\}$, which are zeros of $a(\lambda)$ in the upper complex half-plane together with complex-valued norming constants $\{r_n\}$) [2,3,19]. The discrete eigenvalues correspond to a solitonic part of the field distribution, with N being the total number of solitons in the propagating signal $\Psi_1(T, \tau)$. The knowledge of all the nonlinear spectral parameters (including norming constants) allows us to recover the field $\Psi_1(T, \tau)$ for any T and τ. The nonlinear spectrum evolves trivially with T in the integrable systems; however, in the nonintegrable case, this is not the case, as it will be shown below.

Further we solve numerically Eqs. (2) and (3) and use the obtained data for nonlinear spectrum computation. Figure 1 presents an example of the nonlinear spectrum computed by the contour integral method [20] [shown in Fig. 1(c)] for a single dissipative soliton (here Fig. 1(a) depicts power $|\Psi_1(T = 30, \tau)|^2$, and Fig. 1(b), the Fourier spectrum of the formed soliton $|\Psi_1(T = 30, \omega)|^2$), at the point $T = 30$, generated from the initial conditions with $\Psi_0(T = 0) = 0$, $\Psi_1(\tau, T = 0) = \mathrm{sech}(\tau)$. Stable stationary solutions for Ψ_0 for the considered parameters $\zeta_0 = 2$, $f = \sqrt{2}$ are $\Psi_0 = 1$ and $\Psi_0 = 2$, respectively. With the chosen initial condition $\Psi_0(T = 0) \equiv 0$, the background evolves to $\Psi_0 \equiv 1$ (this is the case for all cases considered in this Letter). Nonlinear discrete spectrum in this case has two eigenvalues.

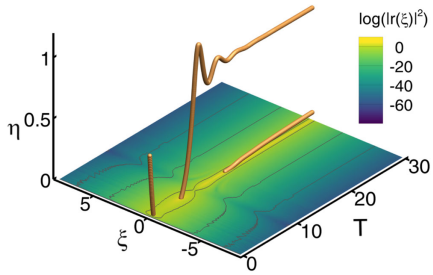

Fig. 2. Dynamics of the nonlinear spectrum for the same conditions as in Fig. 1 shown as the evolution with T in the complex plane $\lambda = \xi + i\eta$: the discrete spectrum (upper part) and the logarithm of $|r(\xi)|^2$ for continuous spectrum (counterplot).

Figure 2 illustrates evolution of the nonlinear spectrum with T in the complex plane $\lambda = \xi + i\eta$, including both discrete eigenvalues and the continuous spectrum. It is seen that during the first stage a single discrete eigenvalue corresponding to the initial condition with the NLSE soliton is destroyed by dissipative and conservative deviations R from the integrable model and all energy is in the continuous spectrum. However, near $T \approx 6$, a generation of a new (dissipative) soliton starts. During the next period after several oscillations, an asymptotic dissipative soliton is formed that can be characterized with good accuracy by just two discrete eigenvalues. Note, that for the NLSE, the total field energy $E_t(T) = \int_{-\infty}^{\infty} |\Psi_1(T, \tau)|^2 d\tau$ can be presented as a sum of a discrete (solitons) $E_d(T)$ and a continuous (dispersive waves) $E_c(T)$ spectra,

$$E_t = E_d + E_c = \sum_{n=1}^{N} 4\eta_n + \frac{1}{\pi}\int_{-\infty}^{\infty} \log(1 + |r(\xi)|^2)d\xi. \tag{6}$$

We stress that we do not aim here to solve underlying equations, but rather to use NFT for signal processing and present temporal signal in a basis with less effective degrees of freedom compared to conventional Fourier presentation. The logic behind this approach is that though LLE is a dissipative and nonintegrable model, in its core there is an integrable NLSE [left-hand side of Eq. (3)]. Therefore, NLSE-based techniques might be inherently useful for analysis of the LLE solutions. In particular, localized coherent structures that are not solutions of NLSE still can be well presented by just a few discrete eigenvalues.

Figure 3 complements Figs. 1 and 2 and demonstrates in more detail how discrete eigenvalues can be used to characterize the coherent structure: Fig. 3(a) shows building of the stable background from initial zero condition; Fig. 3(b) depicts 3D evolution of the solution of Eq. (1) $\Psi_1(\tau, T)$ during the building of a single dissipative soliton. Figure 3(c) presents dynamics with T of the discrete spectrum—the initial single

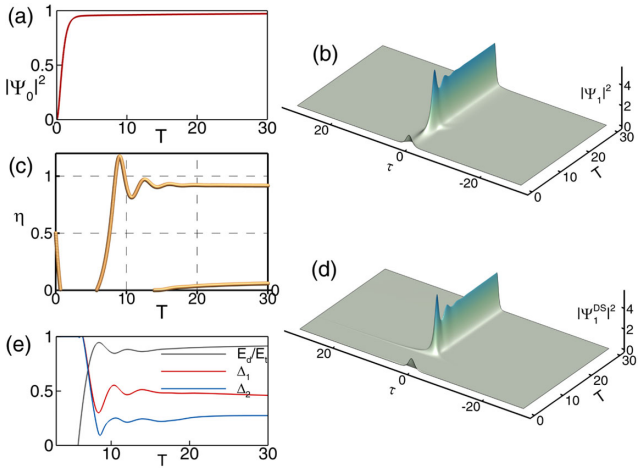

Fig. 3. (a) Transition of the field $\Psi_0(T)$ to stationary asymptotic value $|\Psi_0|^2 = 1$; (b) 3D plot of the generation of a stable dissipative soliton, solution of Eq. (1); (c) nonlinear discrete spectrum evolution with T; (d) dynamics of the field $\Psi_1^{(DS)}(\tau, T)$ reconstructed by the nonlinear discrete spectrum shown in (c) at each point in T; (e) black curve shows evolution with T ($T > 3$) of the fraction of the energy containing in the discrete nonlinear spectrum $E_d(T)$ to the total energy $E_t(T)$; red line corresponds to the relative integral L_2-norm of the difference between the field Ψ_1 and the field $\Psi_1^{(DS)}$ reconstructed from the nonlinear discrete spectrum (c); blue line is similar to the red one, but for the difference between the amplitudes of $|\Psi_1|$ and the reconstructed field $|\Psi_1^{(DS)}|$. Here are the same parameters and initial conditions as in Fig. 1.

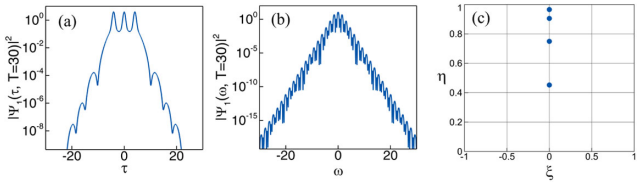

Fig. 4. Solution of LLE for $\varsigma_0 = 2$, $f = \sqrt{2}$, with $\Psi_0(T = 0) = 0$, and $\Psi_1(\tau, T = 0) = 4\,\mathrm{sech}(\tau)$: (a) intensity profile, (b) soliton power spectrum, (c) nonlinear discrete spectrum of the formed train of solitons at $T = 30$.

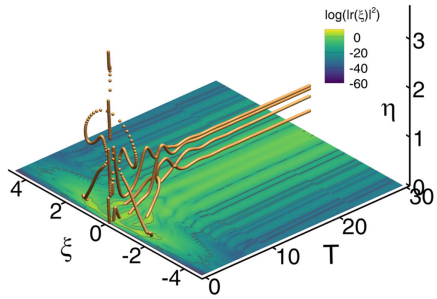

Fig. 5. Same parameters and initial condition as in Fig. 4. Dynamics of the nonlinear spectrum in the complex plane $\lambda = \xi + i\eta$: the discrete spectrum (upper) and the logarithm of $|r(\xi)|^2$ for continuous spectrum (counterplot).

eigenvalue related to the soliton NLSE disappears due to perturbations imposed by R, and at the time $T \approx 6$ corresponding to the formation of a stable dissipative soliton, a new eigenvalue appears, following later by the second one with a lower amplitude. These two eigenvalues characterize the formed dissipative soliton with good accuracy. This is illustrated by the reconstruction of the dissipative soliton 3D evolution from just the two eigenvalues and the corresponding norming constants as shown in Fig. 3(d) (here we neglect the continuous spectrum). It is seen a good agreement with the original field in Fig. 3(b). Figure 3(e) further quantifies the reconstruction: the black line corresponds to the energy fraction contained in the discrete nonlinear spectrum $E_d(T)/E_t(T)$; the red line depicts the evolution of the relative integral L_2-norm difference between the original field and is recovered using the discrete nonlinear spectrum defined as $\Delta_1(T) = [\int |\Psi_1(\tau, T) - \Psi_1^{(DS)}(\tau, T)|^2 d\tau / \int |\Psi_1(\tau, T)|^2 d\tau]^{1/2}$; the blue curve is for $\Delta_2(T) = [\int ||\Psi_1(\tau, T)| - |\Psi_1^{(DS)}(\tau, T)||^2 d\tau / \int |\Psi_1(\tau, T)|^2 d\tau]^{1/2}$.

Next, we consider more complex examples and outline the potential and challenges in signal processing of such structures using NFT. Figure 4 shows the signal formed from the initial conditions $\Psi_0(T = 0) = 0$, $\Psi_1(\tau, T = 0) = 4\mathrm{sech}(\tau)$ (in this case, $\Psi_0(T)$ also evolves into $|\Psi_0(T)| = 1$): Fig. 4(a) depicts a power distribution $|\Psi_1(T = 30, \tau)|^2$ at $T = 30$; Fig. 4(b) depicts a Fourier spectrum of the formed soliton $|\Psi_1(T = 30, \omega)|^2$). The nonlinear discrete spectrum in this case has four eigenvalues [Fig. 4(c)].

Figure 5 shows 3D evolution of the nonlinear spectrum with T in the complex plane $\lambda = \xi + i\eta$, including both the discrete and the continuous spectrum during formation of a set of dissipative solitons on the stable background from the initial distribution $\Psi_1(\tau, T = 0) = 4\,\mathrm{sech}(\tau)$. Formed three dissipative solitons can be characterized by four discrete eigenvalues. Corresponding nonlinear continuous spectrum plays a role at the first stage, but during further evolution, most of the energy moves to the discrete spectrum.

A comparison of the directly computed solution of Eq. (3) and a field reconstructed continuously with T from the nonlinear discrete spectrum [four eigenvalues shown in Fig. 4(c)] is presented in Fig. 6. Namely, Fig. 6(a) shows the 3D evolution of solution of Eq. (3) $\Psi_1(\tau, T)$ in the plane (τ, t), and Fig. 6(b) presents the field reconstructed only from the nonlinear discrete spectrum $\Psi_1^{(DS)}(\tau, T)$. It is seen that despite rather nontrivial multisoliton dynamics, especially at the beginning, four eigenvalues give a relatively good approximation of the complex evolution.

Figure 7 quantifies the process of reconstruction. The black line in Fig. 7 shows evolution with T of the ratio of the energy, which is contained in the discrete nonlinear spectrum to the total energy $E_d(T)/E_t(T)$. It is seen that a lion fraction of the energy, after an initial transition interval, is in the discrete nonlinear spectrum. This makes it possible to describe rather complex dynamics of the solution of the (nonintegrable) nonlinear partial differential equation with good accuracy by only several effective degrees of freedom represented by the parameters of discrete eigenvalues. Integral accuracy of the approximation is characterized by the L_2-norm. Namely, a red line in Fig. 7 corresponds to the relative L_2-norm of the difference between original field Ψ_1 and the field $\Psi_1^{(DS)}$ reconstructed from the discrete spectrum shown in Fig. 5. The blue line in Fig. 7 is similar to the red one, but for the difference between the

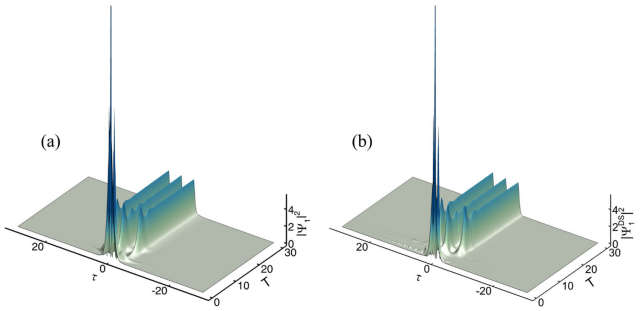

Fig. 6. Same parameters and initial condition as in Fig. 4: (a) numerical solution of Eq. (1) showing building up of the asymptotic set of dissipative solitons–intensity in the plane (τ, T); (b) similar dynamics of the field reconstructed only from the four nonlinear discrete eigenvalues shown in Fig. 4(c).

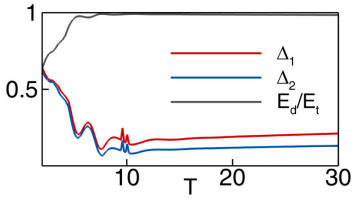

Fig. 7. Black line, evolution with T $(T > 2)$ of the ratio $E_d(T)/E_t(T)$ (black curve); relative integral L_2-norm of the difference between the field Ψ_1 computed in Eq. (3) and the field $\Psi_1^{(DS)}$ reconstructed from the nonlinear discrete spectrum (red line); blue line is similar to the red one, but for the difference between the amplitudes of $|\Psi_1|$ and the reconstructed field $|\Psi_1^{(DS)}|$. Here are the same parameters and initial conditions as in Fig. 4.

amplitudes of the original field $|\Psi_1|$ and the reconstructed field $|\Psi_1^{(DS)}|$.

Note that reconstruction of a complex field with a nonlinear spectrum containing a large number of discrete eigenvalues might technically be challenging. Advanced numerical methods for multisoliton solutions are actively developing now in the context of the integrable turbulence (see for details [21–24]). We anticipate that new effective algorithms will be available for future NFT software toolboxes to make it a routine technique for analysis of experimental data. Analysis of the experimental data with NFT requires consideration of the normalization choice as discussed in detail in a recent paper [6].

In conclusion, using the mean-field master model governing the evolution of optical combs in optical fiber- or microresonators, we demonstrated how the NFT based on the Zakharov–Shabat spectral problem can be applied to characterize generation and propagation of the coherent structures in the case of a stable background. We have shown that the NFT-based approach makes it possible to reduce the number of effective degrees of freedom in situations when the dynamic is dominated by the formation of coherent structures. The developed technique offers a natural framework for the analysis of localized (in time) pulses embedded in the stable CW background. The approach can be extended to the periodic boundary conditions, though many mathematical challenges have to be addressed (see recent applications of periodic NFT in the context of optical communications [25,26]).

Funding. Russian Science Foundation (17-72-30006); Engineering and Physical Sciences Research Council (EP/R035342/1).

Disclosures. The authors declare no conflicts of interest.

REFERENCES

1. C. S. Gardner, J. M. Greene, M. D. Kruskal, and R. M. Miura, Phys. Rev. Lett. **19**, 1095 (1967).
2. V. E. Zakharov and A. B. Shabat, J. Exp. Theor. Phys. **34**, 62 (1972).
3. M. J. Ablowitz, D. J. Kaup, A. C. Newell, and H. Segur, Stud. Appl. Math. **53**, 249 (1974).
4. S. Sugavanam, M. Kamalian, J. Peng, J. E. Prilepsky, and S. K. Turitsyn, in *Conference on Lasers and Electro-Optics Europe & European Quantum Electronics Conference (CLEO/Europe-EQEC)* (IEEE, 2017), Vol. **472**, p. 1.
5. P. Ryczkowski, M. Närhi, C. Billet, J.-M. Merolla, G. Genty, and J. M. Dudley, Nat. Photonics **12**, 221 (2018).
6. S. Sugavanam, M. K. Kopae, J. Peng, J. E. Prilepsky, and S. K. Turitsyn, Nat. Commun. **10**, 5663 (2019).
7. I. S. Chekhovskoy, O. V. Shtyrina, M. P. Fedoruk, S. B. Medvedev, and S. K. Turitsyn, Phys. Rev. Lett. **122**, 153901 (2019).
8. S. Coen, H. G. Randle, T. Sylvestre, and M. Erkintalo, Opt. Lett. **38**, 37 (2013).
9. K. Vahala, Nature **424**, 839 (2003).
10. T. J. Kippenberg, A. L. Gaeta, M. Lipson, and M. L. Gorodetsky, Science **361**, eaan8083 (2018).
11. L. Lugiato, F. Prati, M. L. Gorodetsky, and T. J. Kippenberg, Philos. Trans. R. Soc. London, Ser. A **376**, 20180113 (2018).
12. E. P. Grelu, *Nonlinear Optical Cavity Dynamics: From Microresonators to Fiber Lasers* (Wiley, 2015).
13. I. V. Barashenkov and Y. S. Smirnov, Phys. Rev. E **54**, 5707 (1996).
14. T. Hansson, D. Modotto, and S. Wabnitz, Phys. Rev. A **88**, 023819 (2013).
15. T. Hansson and S. Wabnitz, Nanophotonics **5**, 231 (2020).
16. N. Bekki and K. Nozaki, in *Dynamical Problems in Soliton Systems*, S. Takeno, ed., Springer Series in Synergetics (Springer, 1985), Vol. **30**, p. 268.
17. L. A. Lugiato and R. Lefever, Phys. Rev. Lett. **58**, 2209 (1987).
18. M. Haelterman, S. Trillo, and S. Wabnitz, Opt. Commun. **91**, 401 (1992).
19. S. K. Turitsyn, J. E. Prilepsky, S. T. Le, S. Wahls, L. L. Frumin, M. Kamalian, and S. A. Derevyanko, Optica **4**, 307 (2017).
20. A. Vasylchenkova, J. E. Prilepsky, and S. K. Turitsyn, Opt. Lett. **43**, 3690 (2018).
21. S. Randoux, P. Suret, A. Chabchoub, B. Kibler, and G. El, Phys. Rev. E **98**, 022219 (2018).
22. A. A. Gelash and D. S. Agafontsev, Phys. Rev. E **98**, 042210 (2018).
23. A. Gelash, D. Agafontsev, V. Zakharov, G. El, S. Randoux, and P. Suret, Phys. Rev. Lett. **123**, 234102 (2019).
24. R. Mullyadzhanov and A. Gelash, Opt. Lett. **44**, 5298 (2019).
25. M. Kamalian, J. E. Prilepsky, S. T. Le, and S. K. Turitsyn, Opt. Express **24**, 18353 (2016).
26. M. Kamalian, A. Vasylchenkova, D. Shepelsky, J. E. Prilepsky, and S. K. Turitsyn, J. Light. Technol. **36**, 5714 (2018).